Formation of the pseudoscalars π^0, η, and η' in the reaction $\gamma\gamma \to \gamma\gamma$

D. A. Williams,[t,β] D. Antreasyan,[t] H. W. Bartels,[ε] D. Besset,[λ] Ch. Bieler,[θ] J. K. Bienlein,[ε]
A. Bizzeti,[η] E. D. Bloom,[μ] I. Brock,[γ] K. Brockmüller,[ε] R. Cabenda,[λ] A. Cartacci,[η] M. Cavalli-Sforza,[λ,β]
R. Clare,[μ,(a)] A. Compagnucci,[η] G. Conforto,[η] S. Cooper,[μ,(a)] R. Cowan,[λ,(a)] D. Coyne,[λ,β] G. Drews,[ε]
A. Engler,[γ] K. H. Fairfield,[μ] G. Folger,[ς,(b)] A. Fridman,[μ,(i)] J. Gaiser,[μ] D. Gelphman,[μ] G. Glaser,[ς]
G. Godfrey,[μ] F. H. Heimlich,[θ,η] R. Hofstadter,[μ] J. Irion,[t] Z. Jakubowski,[δ] K. Karch,[ν] S. Keh,[ν,(c)]
H. Kilian,[ν] I. Kirkbride,[μ] T. Kloiber,[ε] M. Kobel,[ς] W. Koch,[ε] A. C. König,[κ] K. Königsmann,[ν]
R. W. Kraemer,[γ] S. Krüger,[θ] G. Landi,[η] R. Lee,[μ] S. Leffler,[μ] R. Lekebusch,[θ] W. Lockman,[μ,(d)]
S. Lowe,[μ] B. Lurz,[ς] D. Marlow,[γ,λ] H. Marsiske,[ε] W. Maschmann,[θ] P. McBride,[t] F. Messing,[γ]
W. J. Metzger,[κ] H. Meyer,[ε] B. Monteleoni,[η] R. Nernst,[θ] B. Niczyporuk,[μ] G. Nowak,[δ] C. Peck,[α]
P. G. Pelfer,[η] B. Pollock,[μ] F. C. Porter,[α] D. Prindle,[γ] P. Ratoff,[α,(e)] M. Reidenbach,[κ] B. Renger,[γ]
C. Rippich,[γ] M. Scheer,[ν] P. Schmitt,[ν,t] J. Schotanus,[κ] J. Schütte,[ς] A. Schwarz,[μ,(f)] F. Selonke,[ε]
D. Sievers,[θ] T. Skwarnicki,[ε] V. Stock,[θ] K. Strauch,[t] U. Strohbusch,[θ] J. Tompkins,[μ,(g)] H. J. Trost,[ε,(f)]
R. T. Van de Walle,[κ] H. Vogel,[γ] A. Voigt,[ε] U. Volland,[ς] K. Wachs,[ε] K. Wacker,[μ,(h)] W. Walk,[κ,(c)]
H. Wegener,[ς] and P. Zschorsch[ε]

[a]*California Institute of Technology, Pasadena, California 91125*
[β]*University of California, Santa Cruz, California 95064*
[γ]*Carnegie-Mellon University, Pittsburgh, Pennsylvania 15213*
[δ]*Cracow Institute of Nuclear Physics, Cracow, Poland*
[ε]*Deutsches Electronen Synchrotron DESY, Hamburg, Germany*
[ς]*Universität Erlangen-Nürnberg, Erlangen, Germany*
[η]*Istituto Nazionale di Fisica Nucleare and University of Firenze, Firenze, Italy*
[θ]*Universität Hamburg, I. Institut für Experimentalphysik, Hamburg, Germany*
[t]*Harvard University, Cambridge, Massachusetts 02138*
[κ]*University of Nijmegen and Nationaal Instituut voor Kernfysica en Hoge-Energiefysica–Nijmegen, Nijmegen, The Netherlands*
[λ]*Princeton University, Princeton, New Jersey 08544*
[μ]*Department of Physics, High Energy Physics Laboratory, and Stanford Linear Accelerator Center,
Stanford University, Stanford, California 94305*
[ν]*Universität Würzburg, Würzburg, Germany*
(The Crystal Ball Collaboration)
(Received 4 April 1988)

The Crystal Ball detector has been used at the DORIS II storage ring at DESY to study the reaction $e^+e^- \to e^+e^-\gamma^*\gamma^* \to e^+e^-X \to e^+e^-\gamma\gamma$, where X is a narrow resonance with mass between 100 and 3000 MeV. Formation of π^0, η, and η' mesons is observed, and the following meson partial widths are obtained: $\Gamma_{\pi^0 \to \gamma\gamma} = 7.7 \pm 0.5 \pm 0.5$ eV, $\Gamma_{\eta \to \gamma\gamma} = 0.514 \pm 0.017 \pm 0.035$ keV, and $\Gamma_{\eta' \to \gamma\gamma} = 4.7 \pm 0.5 \pm 0.5$ keV. No other narrow resonances are observed, and upper limits are given for the product $\Gamma_{X \to \gamma\gamma} B_{X \to \gamma\gamma}$.

I. INTRODUCTION

Photon-photon production of neutral resonances provides important information about the constituents of the resonance. Photons cannot couple to a neutral particle directly, but must interact with charged constituents or via intermediate virtual charged particles. In the quark model of mesons, the strength of the coupling is related to the quark content. An important check of whether a resonance is a conventional $q\bar{q}$ meson is a comparison of its measured partial width $\Gamma_{X \to \gamma\gamma}$ with the quark-model prediction based on its quark composition determined from other types of measurements.

For the light pseudoscalars π^0, η, and η', the two-photon partial widths are also of interest as a determination of their lifetimes. These particles have lifetimes in

the range 10^{-21}–10^{-16} sec which is difficult to measure: they have both a short decay length and a small natural width. The best determinations of the η and η' lifetimes are obtained by using measurements of $\Gamma_{X \to \gamma\gamma}$ and the branching ratio for $X \to \gamma\gamma$ to derive the full width.[1] A precise measurement of the π^0 lifetime using the decay-length technique was recently achieved by Atherton *et al.*[2]

In this paper we describe a study[3] of the reaction $e^+e^- \to e^+e^-\gamma^*\gamma^* \to e^+e^-\gamma\gamma$, where each γ^* is a quasireal photon radiated from one of the beam particles. The virtual photons scatter to produce a final state consisting of two real photons. The final-state leptons scatter at very small angles and are not detected. The sum of the transverse momenta of the final-state photons with respect to the beam axis is essentially zero. We observe three peaks in the invariant-$\gamma\gamma$-mass spectrum corresponding to the formation of π^0, η, and η' mesons. This is the first observation of π^0 production using this technique, first suggested by Low[4] in 1960.

The data used for this analysis were collected with the Crystal Ball detector running at the DORIS II e^+e^- storage ring at DESY. The e^+e^- center-of-mass energy varied from 9.4 to 10.6 GeV, with most of the data taken on the $\Upsilon(1S)$, $\Upsilon(2S)$, and $\Upsilon(4S)$ resonances. The sample used for the study of η and η' production has an integrated luminosity of 114 pb^{-1}, of which about 40% has trigger thresholds also suitable for the π^0 study. A sample of single-beam and separated-beam data corresponding to approximately 6 pb^{-1} of colliding-beam data has been used to study beam-gas backgrounds.

II. DETECTOR AND TRIGGER

The Crystal Ball detector has been described in some detail before.[5] The ball consists of an array of 672 NaI(Tl) crystals covering 93% of the solid angle with a thickness of 15.7 radiation lengths. The light produced in each crystal is detected by one photomultiplier. The crystals are stacked to form a hollow sphere centered at the interaction region (see Fig. 1). The arrangement is based on an icosahedron in which each face has been subdivided into 36 smaller triangles. The group of 36 crystals associated with one face of the icosahedron is called a "major triangle." A full sphere would contain 720 crystals. To allow the beam pipe to pass through the ball, there are two openings, each of which results from omitting a group of 24 crystals. The two sets of 30 crystals adjacent to the openings are called the "tunnel regions," and the crystals not in the tunnel regions are called the "main ball."

The measured energy resolution of the Crystal Ball for electromagnetically showering particles is $\sigma_E/E = (2.7 \pm 0.2)\%/E^{1/4}$ (E in GeV), with the energy shared among a symmetric cluster of 13 neighboring crystals. Using the distribution of energy within the cluster, we determine the direction of showering particles to an accuracy ranging from about 3° for the polar angle of a 70-MeV photon to about 2° at 500 MeV. The NaI(Tl) energy scale is determined using large-angle Bhabha scattering events. We use our studies of the $\Upsilon(2S) \to \pi^0\pi^0\Upsilon(1S)$
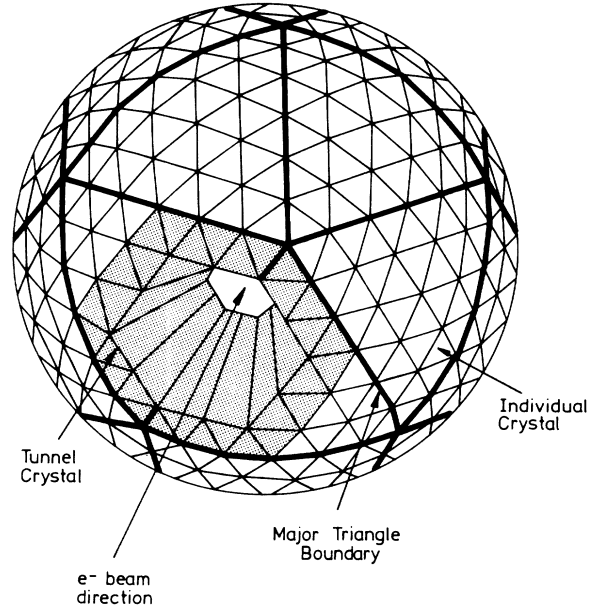

FIG. 1. The organization of the Crystal Ball into major triangles. The shaded area is one of the "tunnel regions" next to the beam.

channel to correct the calibration at lower energies by a one-parameter, nonlinear expression,[6] which gives a correction of +5% at 100 MeV.

The ball is augmented by NaI(Tl) end caps which cover an additional 5% of the solid angle with an average thickness of about 8 radiation lengths. For the present analysis, the end caps are not used to reconstruct events. However, they are used to identify and reject events which are not fully contained in the ball.

The central cavity of the ball is equipped with proportional wire chambers to detect charged particles. The chambers consist of individual aluminum tubes arranged in cylindrical double layers around the beam pipe, with one layer offset from the other by half of the tube spacing. The azimuthal angle ϕ of a hit is determined by the position of the tube that is hit. The pulse at each end of the sense wire is measured, and the position of the hit in the z direction, the direction along the beam axis, is determined by charged division. The resolution in z is roughly 2% of the tube length, which varies from 64.8 to 36.8 cm with increasing distance from the beam pipe.

Two sets of chambers have been used at DORIS. The old set consisted of three double layers of tubes that had walls 75 μm thick, operated using "magic gas." The new set has four double layers and 180-μm-thick walls and was operated using a mixture of 79% argon, 20% CO_2, and 1% methane. For the first part of the data sample used in this analysis, the inner two double layers of the new set and the outer double layer of the old set were installed. For the later data, the complete new set of chambers was installed. The beam pipe has a thickness corresponding to 0.017 radiation lengths (r.l.). Each old double-layer chamber adds 0.010 r.l., whereas a new double layer adds 0.017 r.l.

To help recognize cosmic-ray events, there is an array of 94 plastic scintillation counters ("roof counters") above the ball at a distance of about 3 m from the beam axis.[7] The counters cover about 1π solid angle and intercept about 80% of the triggered cosmic rays that pass through the ball. Their time resolution is about 1 nsec, and the position along the counter is determined with an accuracy of about 20 cm.

The triggers used for this analysis are based on fast analog sums of the energy deposited in the main ball, each of its major triangles, and the tunnel regions. Energy is deposited in the tunnel regions more often than in the rest of the ball, partly because beam-gas and beam-wall collisions that occur outside the central cavity of the ball can produce particles that enter the ball through the tunnel crystals. For this reason, energy in the tunnel regions is excluded from the major-triangle and main-ball energy sums, giving an effective trigger solid angle of 85% of 4π. The energy sums are subjected to both pulse height and constant fraction discriminators. The constant fraction discriminators serve to record the time of arrival of the energy pulse. The trigger decisions are based on logical combinations of the pulse-height discriminator outputs, all of which are recorded on tape for each triggered event. By examining events which satisfied more than one trigger, the threshold and efficiency can be determined for each discriminator. Based on the hardware thresholds measured in this way, we set sharp software thresholds safely above the measured values (below for vetoes). Events used in the analysis presented here are required to satisfy these software thresholds, which are given in the following trigger description.

In order to detect a single π^0 or η produced nearly at rest, a trigger with a low energy threshold is required. We have used two triggers for this analysis. One, which we refer to as the "π^0 trigger," requires at least 90 MeV in the main ball. The other, the "η trigger," requires at least 400 MeV. To reduce background contributions to the trigger rate to manageable levels, additional constraints on the events are required, as described below.

A topology requirement is the main test applied by both the π^0 trigger and the η trigger. It was specifically designed to accept candidates for $\gamma\gamma$ collision events, making use of the fact that most such events have nearly balanced transverse momentum. Any plane that contains the beam axis divides the ball into two hemispheres. If one of the hemispheres contains all of the energy in the event and the other is empty, then it is not possible that the event balances transverse momentum. The trigger uses three such planes to divide the ball into a total of six hemispheres. The hemisphere boundaries are chosen to coincide with the major-triangle boundaries, resulting in imperfect hemispheres. The major-triangle energy sums are used to determine which hemispheres are occupied. For the π^0 trigger, the major-triangle threshold is set to 45 MeV; the η trigger requires 160 MeV in a major triangle. If the threshold is exceeded, the major triangle and any hemisphere containing it are considered hit. For the topology requirement to be met, each of the six hemispheres must have at least one such hit. Although there

are six hemispheres, as few as two major triangles with energy are enough to set the trigger. Each major triangle is included in three of the hemispheres, and energy in the triangle will satisfy the requirement for all three hemispheres. Roughly speaking, two particles coplanar with the beams are sufficient to satisfy the topology requirement if each sets a major triangle on opposite sides of the beam axis.

Two vetoes are imposed on events to further suppress background from beam-gas events and cosmic-ray events. Both the π^0 trigger and the η trigger make use of a veto on the energy in the two tunnel regions. If the energy in either tunnel region exceeds 30 MeV, the event is vetoed.

The second veto uses the chambers to reject charged particles. The wires in each layer of the chambers are grouped in sets of eight. The pulses from both ends of the eight wires are summed. If any of the sums for a layer exceeds a threshold, that layer is considered hit. The η trigger is vetoed if either layer 5 or 6 has a hit. The π^0 trigger is vetoed if any of layers 3 through 6 are hit. The thresholds are set rather high so that noise hits do not set the veto. Consequently, some charged tracks are not vetoed. Roughly 10% of Bhabha events do not set the chamber veto.

The π^0 trigger and η trigger make use of the same hardware with different threshold settings, so they cannot be run simultaneously. With the exception of the slightly more rigorous chamber veto, the π^0 trigger accepts all events that the η trigger would accept. The data used here consist of 68 pb^{-1} with the η trigger and 46 pb^{-1} with the π^0 trigger.

III. EVENT SELECTION

Events satisfying the π^0 trigger or η trigger are passed through a preliminary selection designed to identify candidates for events produced by photon-photon collisions. This selection requires events to have total energy in the ball less than 5 GeV and net transverse momentum[8] $|\sum \mathbf{p}_t|$, less than 200 MeV.

From this sample of photon-photon collision candidates we select events in which the final state consists of two photons. The analysis covers a large range of $\gamma\gamma$ invariant mass and has been separated into a low-mass and high-mass region. The low-mass analysis uses only the data with the π^0 trigger and has been used to measure π^0 production and obtain upper limits for states with mass between the π^0 and η mass. The high-mass analysis uses the combined sample of π^0-trigger and η-trigger data to study η and η' production and to search for states with mass larger than 600 MeV. As discussed in the previous section, events have been required to satisfy software trigger thresholds which are somewhat more restrictive than the hardware trigger thresholds. Events used in the high-mass analysis are required to satisfy the software thresholds for the η trigger, regardless of whether they are from a run with the π^0 trigger or η trigger. For the most part, the same selection criteria are used for both mass regions. In the following discussion, the requirements are used for the whole mass range unless otherwise noted.

We select events that have two neutral showers, each with a least 40 MeV, and no other tracks or showers with more than 10 MeV. Each shower is required to satisfy $|\cos\theta| \leq 0.75$, where θ is the angle between the direction of the positron beam and the shower direction. The showers are required to have lateral energy deposition consistent with that expected from an electromagnetic shower. For the low-mass region, there is a cleanliness requirement that the total energy in the ball cannot exceed the sum of the energy of the two showers by more than 25 MeV.

Cosmic-ray events can mimic an event with two showers in the ball. If a minimum-ionizing particle passes through the ball by way of the central cavity, it leaves two regions of ionization, each with 150–300 MeV. The roof counters are used to reject the majority of cosmic-ray particles: those which are moving downward and cross the roof counters before passing through the ball. Events with a roof hit recorded more than 5 nsec before the energy deposition in the bottom hemisphere of the ball are rejected. (Showers with at least 130 MeV in the bottom hemisphere needed to set the timing discriminator are measured with a resolution of about 1 nsec. Events with less than this amount of energy are treated as if they had no roof hits.) For the high-mass analysis, the signal in the ball is also required to be consistent with the nominal time of the beam crossing.

The standard tracking algorithms, which are used to identify and reject events with charged particles, assume that tracks originate from the beam crossing. For beam-gas events and cosmic rays this is not necessarily true, so two additional requirements have been used to eliminate such events. In the first, events with hits in the chambers closely matched in ϕ (the azimuthal angle around the beam axis) to the direction of either of the photon candidates are rejected. Here we ignore the z information since beam-gas tracks can originate anywhere along the beam axis. The second requirement rejects cosmic-ray events by identifying the straight track they produce through the chambers. Again ignoring the z information, if a line of chamber hits can be found that passes close to a crystal from each shower containing at least 10 MeV, the event is rejected.

Events produced by photon-photon collisions are expected to have very small total transverse momentum. Figure 2 shows the $\gamma\gamma$ invariant-mass distributions for events with $|\sum \mathbf{p}_t| \leq \frac{1}{10}M_{\gamma\gamma}$. Clear signals are seen at the π^0, η, and η' masses. To verify that these mass peaks indeed arise from events with balanced transverse momentum, the distribution of $|\sum \mathbf{p}_t|^2$ before the cut is shown in Fig. 3 for the neighborhood of each of the peaks. The distributions peak at small transverse momentum, as expected, and are consistent with the Monte Carlo expectation for the shape of the transverse-momentum distribution plus a background that is approximately flat. Only the events with $|\sum \mathbf{p}_t| \leq \frac{1}{10}M_{\gamma\gamma}$ are kept. To further reduce background contributing to the π^0 and η peaks, the π^0 and η signals are determined using only events which also satisfy $|\sum \mathbf{p}_t| \leq 10$ MeV and $|\sum \mathbf{p}_t| \leq 45$ MeV, respectively.
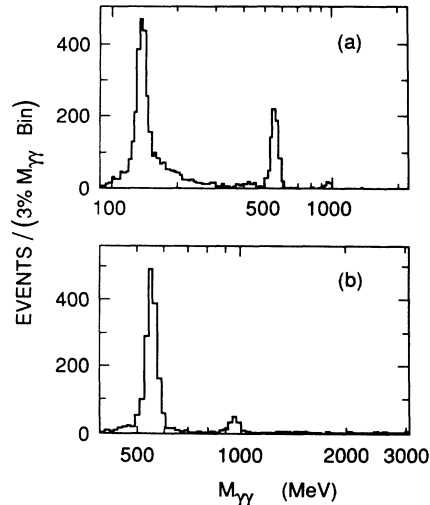

FIG. 2. The $M_{\gamma\gamma}$ distribution for events selected as described in the text and which have $|\sum \mathbf{p}_t| \leq \frac{1}{10}M_{\gamma\gamma}$. (a) shows the distribution for events satisfying the low-mass selection; (b) shows the data sample for the high-mass analysis.

IV. BACKGROUND ESTIMATES

To determine the partial width of each of the observed pseudoscalars, we need to know how many of the events in each signal are actually due to the process

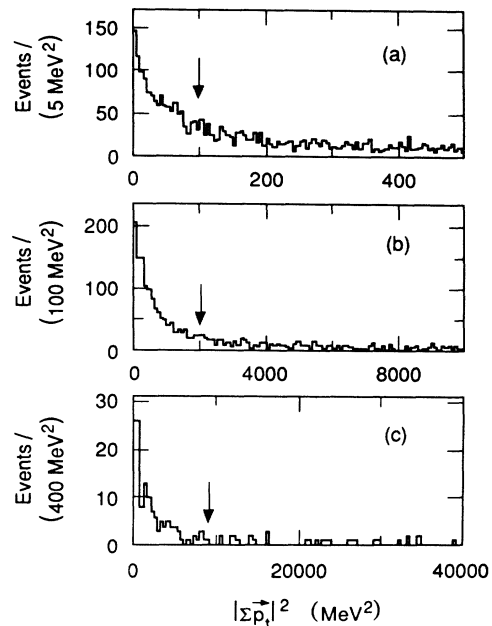$$e^+e^- \rightarrow e^+e^-X, \quad X \rightarrow \gamma\gamma . \tag{1}$$

FIG. 3. The $|\sum \mathbf{p}_t|^2$ distribution in the neighborhood of each of the peaks in the invariant-mass distribution: (a) for $125 \leq M_{\gamma\gamma} \leq 145$ MeV; (b) for $500 \leq M_{\gamma\gamma} \leq 600$ MeV; (c) for $900 \leq M_{\gamma\gamma} \leq 1000$ MeV. Note the different scales on the horizontal axes. It is conventional to plot $|\sum \mathbf{p}_t|^2$ because background from beam-gas or incompletely contained events tends to produce a flat distribution in this quantity. The arrows indicate the cuts used to obtain the events in Figs. 5–7.

Some background processes, such as e^+e^- $\rightarrow e^+e^-e^+e^-$, where the tracks associated with the e^+ and e^- showers fail to be identified, produce background distributed smoothly as a function of invariant mass. Backgrounds of this type are accounted for by fitting the mass distribution with peaks plus a smooth function. Estimates of the expected amount of smooth background are consistent with the small amount seen in the data. We will concentrate here on the more troublesome background processes, those which contribute directly to the strength of the observed signals. These are processes in which a π^0, η, or η' meson is produced by some mechanism other than (1).

One source of this type of background is beam-gas collisions. The correlation of $\gamma\gamma$ invariant mass and total transverse momentum for e^+e^- collision events satisfying the low-mass selection is shown in Fig. 4(a). The analogous plot is shown in Fig. 4(b) for a sample of beam-gas data satisfying the same selection criteria. The beam-gas data were collected during runs with the e^+ and e^- beam separated at the interaction region, or with a single e^+ or e^- beam. Both the colliding-beam and the beam-gas samples have a band of events at the π^0 mass which extends to large transverse momentum. These events are most likely produced by excitation of baryonic resonances, e.g., $eN \rightarrow e\Delta$, $\Delta \rightarrow \pi^0 N$, where e and N are both undetected. Only in the colliding-beam sample is there a very tight cluster of events at small transverse momentum.

The beam-gas data are used to subtract the beam-gas background bin by bin from the π^0 region of the $\gamma\gamma$ mass distribution. The relative normalization of the two samples has been determined to be 7.7 ± 0.7 using events with $M_{\gamma\gamma} \leq 200$ MeV and $|\sum \mathbf{p}_t| \geq 20$ MeV. Figure 5 shows the mass distribution for the colliding-beam data together with the normalized beam-gas data. The error bars for

FIG. 5. Events near the π^0 mass which have $|\sum \mathbf{p}_t| \leq 10$ MeV. The colliding-beam data are shown as a histogram and the beam-gas data as points with error bars. The beam-gas data have been multiplied by the normalization factor 7.7

the beam-gas data reflect only the normalized statistical error. The error for the normalization factor is taken into account as described in Sec. V. The mass spectrum after beam-gas subtraction is shown in Fig. 7(a).

In contrast to the π^0 region, there are few events in the beam-gas sample near the η mass. Figure 6 shows the beam-gas events satisfying the high-mass selection and having $|\sum \mathbf{p}_t| \leq 45$ MeV. There is little indication of an enhancement in the η mass region. A fit to the histogram with a linear function plus a peak with mass and width matching the observed η peak in the colliding-beam data yields $0.3^{+2.0}_{-0.3}$ events in the peak. The normalization of the total colliding-beam sample used in the high-mass analysis to the beam-gas sample has been estimated using the factor of 7.7 from the low-mass analysis times the ratio of the total luminosity to the luminosity used in the low-mass analysis. The result is that the beam-gas data must be multiplied by 19 to compare to the colliding-beam data. This implies that beam-gas events contribute 6^{+38}_{-6} events to the η peak in the colliding-beam data. This contribution is subtracted from the total number of observed η events.

There are no events in the beam-gas sample with $850 \leq M_{\gamma\gamma} \leq 1050$, even at large total transverse momentum. We conclude that beam-gas background makes a negligible contribution to the η' signal.

Another possible source of signal events is two-photon collision events producing several particles, of which only
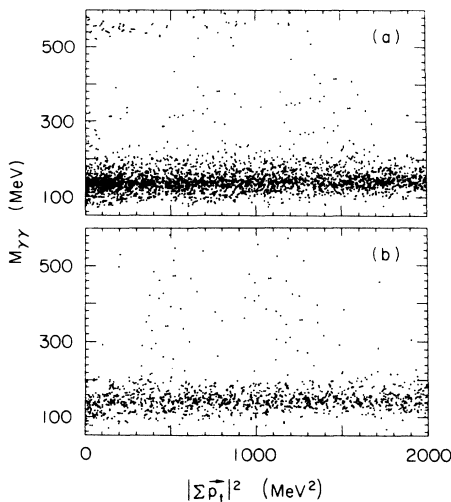

FIG. 4. Correlation of $\gamma\gamma$ invariant mass and transverse momentum for colliding-beam events (a) and beam-gas events (b). To prevent the colliding-beam plot from becoming too dense, only every fourth event has been plotted.
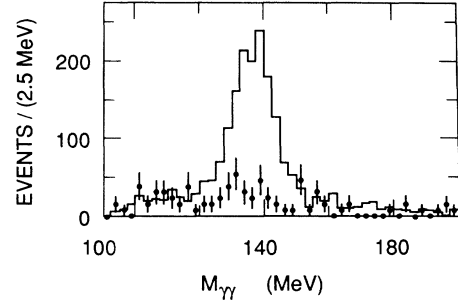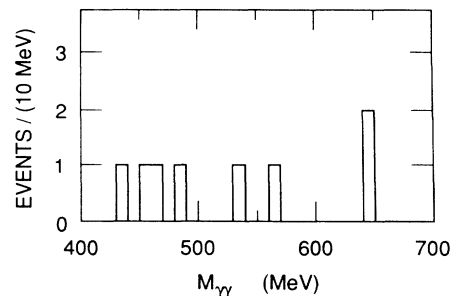

FIG. 6. Invariant-mass distribution for beam-gas events near the η mass and satisfying the high-mass selection.

a single pseudoscalar is observed. The η, η', $a_0(980)$, $f_2(1270)$, and $a_2(1320)$ have all been observed in photon-photon collisions and all have substantial decay modes containing a π^0 or an η (Ref. 1). For the known decays of these particles with branching ratios of a few percent or more, the acceptance for observing only two photons has been studied using Monte Carlo techniques. Only three modes are found which contribute one background event or more. They are

$$\eta \rightarrow \pi^0(\pi^+\pi^-), \quad \pi^0 \rightarrow \gamma\gamma, \quad 1.2\pm0.9 \ \pi^0 \text{ events ;}$$

$$\eta' \rightarrow \eta(\pi^+\pi^-), \quad \eta \rightarrow \gamma\gamma, \quad 11\pm3 \ \eta \text{ events ;}$$

$$a_0(980) \rightarrow \eta(\pi^0), \quad \eta \rightarrow \gamma\gamma \quad (\pi^0 \rightarrow \gamma\gamma) ,$$

$$1.2\pm0.6 \ \eta \text{ events ,}$$

where the particles in parentheses escape detection. These background contributions are subtracted from the number of observed events. Two-photon continuum production of $\pi^0\pi^0$ pairs[9] contributes less than one event and has been neglected.

Monte Carlo studies of e^+e^- annihilation into $q\bar{q}$ pairs or three gluons indicate that background from these sources is negligible.

V. TWO-PHOTON WIDTHS OF THE OBSERVED PSEUDOSCALARS

The number of signal events N in each of the resonance peaks is related to the cross section according to

$$N = \left[\sum_{\text{beam energies}} \epsilon_i \mathcal{L}_i (\sigma_X)_i \right] B_{X \rightarrow \gamma\gamma} , \tag{2}$$

where for each beam energy i, ϵ_i is the detection efficiency, $\mathcal{L}_i$ is the integrated luminosity, $(\sigma_X)_i$ is the cross section for $e^+e^- \rightarrow e^+e^-X$, and $B_{X \rightarrow \gamma\gamma}$ is the branching ratio for X to decay to two photons.

The cross section σ_X for the formation of a particle X in $e^+e^- \rightarrow e^+e^-\gamma^*\gamma^*$, $\gamma^*\gamma^* \rightarrow X$ can be written as

$$\sigma_X = \int \frac{d^3p_1'}{E_1'} \frac{d^3p_2'}{E_2'} \Phi(q_1,q_2) \sigma_{\gamma\gamma \rightarrow X}(q_1,q_2) , \tag{3}$$

where (p_1',E_1') and (p_2',E_2') are the four-vectors of the final state e^+ and e^-, and $\Phi(q_1,q_2)$ describes the production rate of the corresponding virtual photons with four-vectors q_1 and q_2. The cross section for these photons to form a narrow pseudoscalar resonance X is given by[10]

$$\sigma_{\gamma\gamma \rightarrow X}(q_1,q_2) = \Gamma_{X \rightarrow \gamma\gamma} \frac{8\pi^2}{m_X} \delta((q_1+q_2)^2 - m_X^2)$$

$$\times \frac{2|\mathbf{q}|}{m_X} F^2(q_1^2,q_2^2) . \tag{4}$$

The first line is the narrow resonance approximation to the Breit-Wigner cross section for the formation of a spin-0 resonance by two real photons. $\Gamma_{X \rightarrow \gamma\gamma}$ is conventionally defined to be the partial width to real photons, whereas in the two-photon process the photons are slightly virtual $(q^2 < 0)$. We describe the q^2 dependence of $\sigma_{\gamma\gamma \rightarrow X}$ with the second line in Eq. (4). Lorentz and

gauge invariance in QED constrain the form of the $\gamma\gamma$-pseudoscalar vertex,[11] leading to the factor $2|\mathbf{q}|/m_X$, where $\mathbf{q}$ is the momentum of either photon in the X center-of-mass frame. For real photons this factor is 1.

QED does not constrain the form of the electromagnetic form factor $F(q_1^2,q_2^2)$, which depends only on the scalar quantities q_1^2 and q_2^2. It is normalized such that $F(0,0)=1$. Our cut of $|\sum \mathbf{p}_t| \le \frac{1}{10}M_{\gamma\gamma}$ effectively restricts the observed data sample to small[12] q^2, where F is near 1. Therefore, we take $F(q_1^2,q_2^2)=1$ in Eq. (4) above. We have investigated the effect of using the vector-dominance-model (VDM) form factor, $F(q_1^2,q_2^2)=(1 -q_1^2/m_\rho^2)^{-1}(1-q_2^2/m_\rho^2)^{-1}$, where m_ρ is the mass of the ρ meson. This form factor has been shown to give a good description of single-tag production of the η' meson.[13-15] For η' production, the form factor reduces the total cross section $\sigma_{\eta'}$ by 28%. However, the visible η' cross section in the region of phase space accepted by this experiment is only reduced by 0.5%. The effect of the form factor is even less for the π^0 and η.

We use a Monte Carlo event generator based on a program by Vermaseren[16] to calculate $\tilde{\sigma}_X$, the cross section in Eq. (3) with $\Gamma_{X \rightarrow \gamma\gamma}$ set equal to 1 keV. (Consequently, $\tilde{\sigma}_X$ has dimensions nb/keV.) We have neglected the contributions of radiative corrections and e^+/e^- beam transverse polarization. For a no-tag experiment, the effect of transverse beam polarization is vanishingly small.[17] Likewise, radiative corrections have been shown to be less than 1% (Ref. 18). We estimate a systematic error of 2% on $\tilde{\sigma}$, including the effects of the VDM form factor, the radiative corrections, and the averaging technique described below.

The partial width $\Gamma_{X \rightarrow \gamma\gamma}$ can be derived from the number of observed events using Eq. (2). For simplicity, we replace the sum over beam energies by the total luminosity and luminosity-weighted averages of the cross section and detection efficiency. The error that results from this approximation is less than 1%. The detection efficiency ϵ is a product of three efficiencies: ϵ_{ball}, the efficiency for the requirements based on energy deposition in the NaI(Tl); $\epsilon_{\text{chamber}}$, the efficiency for both final-state photons to traverse the tracking chambers without being misidentified as charged particles; and ϵ_{TOF}, the efficiency of the ball and roof timing requirements. The resulting expression for the partial width is

$$\Gamma_{X \rightarrow \gamma\gamma} = \frac{N}{\epsilon_{\text{ball}}\epsilon_{\text{chamber}}\epsilon_{\text{TOF}}\tilde{\sigma}_X \mathcal{L} B_{X \rightarrow \gamma\gamma}} . \tag{5}$$

The number of events in each of the observed peaks has been determined by a fit to the $M_{\gamma\gamma}$ distribution. Each peak region is fit separately with a low-order polynomial background plus a peak of variable mass and width. The energy response of the Crystal Ball is asymmetric with a tail on the low-energy side[19] and produces a similar tail in the invariant-mass distribution of two photons from the decay of a slowly moving particle.[20] We parametrize the peak shape using a Gaussian distribution to which a power-law tail has been joined about 1.3σ below the mean in such a way that the first derivative is continuous. The parameters describing the position
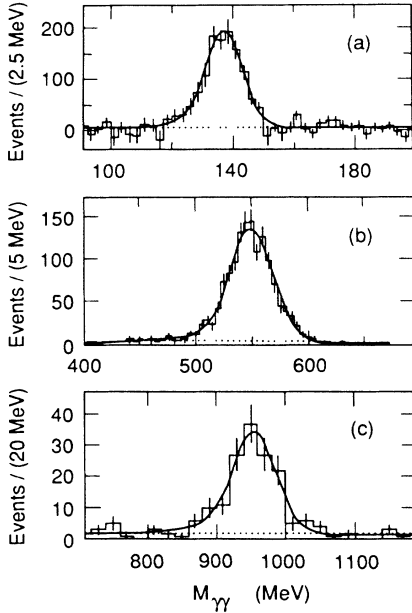
FIG. 7. Fits to the three resonance peaks. The histograms show the number of events satisfying the selection criteria described in Sec. III; in (a) beam-gas events have been subtracted as described in Sec. IV. The smooth curves show the fits described in Sec. V; the dotted curves indicate the background under the peak in each fit.

where the two functions are joined and the power law for the tail are determined by fitting Monte Carlo distributions for $M_{\gamma\gamma}$ from π^0, η, and η' decays. The Monte Carlo showers have been generated using EGS code.[21] The actual data are then fit with the amplitude, mean, and σ free, but the other shape parameters fixed. The fits are shown in Fig. 7. The number of events in each of the peaks is given as N_{fit} in Table I. The first error is statistical and the second error includes the systematic error estimated by varying the fit hypothesis (peak shape and background polynomial). The systematic error for the number of π^0 events consists of an error of ± 12 from the fit hypothesis and ± 22 from the beam-gas normalization

that have been added in quadrature. The error due to the beam-gas normalization factor, 7.7 ± 0.7, has been determined by using normalizations of 7.0 of 8.4 to make the beam-gas subtraction, fitting the resulting $M_{\gamma\gamma}$ distribution, and comparing the result to that obtained using 7.7 for the beam-gas normalization.

The remaining background contributions discussed in the previous section are also shown in Table I. They have been subtracted from the number of events determined by the fits and the errors have been added in quadrature to obtain the number of observed signal events, N.

As for other recent Crystal Ball measurements,[22,23] the luminosity is determined using events with two high-energy showers in the ball from the processes $e^+e^-\rightarrow e^+e^-(\gamma)$ and $e^+e^-\rightarrow\gamma\gamma(\gamma)$. We obtain 46.1 pb^{-1} for the data sample used in the low-mass analysis and 114.0 pb^{-1} for the total sample. We estimate a systematic error of 3% for this procedure. However, part of the data (33.1 pb^{-1}, of which 13.2 pb^{-1} has the low-energy threshold) was taken when some crystals in the detector were being read out improperly.[24] For these data, the number of observed events is somewhat more sensitive to the selection requirements, and we assign a systematic error of 6% for the luminosity from this period. The result is an overall systematic error of 4% for the luminosity, which is shown with the luminosity values in Table I.

We determine the efficiency ϵ_{ball} using Monte Carlo events which have been passed through the EGS detector simulation. The Monte Carlo includes a simulation of the read-out problem,[24] which decreases the detection efficiency for η' events by $(2.5\pm 1.3)\%$ compared to unaffected data. This reduction, together with the fraction of the data which is affected, are taken into account in the final value of ϵ_{ball}. Because the read-out errors were limited to photon energies $\gtrsim 400$ MeV, the effect on the efficiency for π^0 and η events is negligible.

Some of the selection criteria are affected by extra energy deposited in the NaI(Tl) by beam-related backgrounds. This extra energy was measured using a sample of random background events obtained by triggering on every 10^7th beam crossing, with no other condition. Each Monte Carlo event was superimposed on one of the

TABLE I. Numerical values of the quantities involved in the calculation of $\Gamma_{X\rightarrow\gamma\gamma}$. For π^0, N_{fit} is obtained from the mass spectrum after subtracting the beam-gas distribution. For η, the small beam-gas background is included in "Remaining backgrounds."

	π^0	η	η'
N_{fit}	$1183\pm 71\pm 25$	$1313\pm 44^{+50}_{-35}$	$136\pm 14\pm 2$
Remaining backgrounds	1.2 ± 0.9	$(6^{+38}_{-6})+(12\pm 3)$	
N	$1182\pm 71\pm 25$	$1295\pm 44\pm 52$	$136\pm 14\pm 2$
ϵ_{ball}	0.0213 ± 0.0008	0.0491 ± 0.0009	0.0734 ± 0.0026
$\epsilon_{chamber}$	0.707 ± 0.017	0.660 ± 0.015	0.655 ± 0.015
ϵ_{tof}		0.984 ± 0.003	0.995 ± 0.001
$\bar{\sigma}_X$	223.7 ± 4.5 nb/keV	1.78 ± 0.04 nb/keV	0.239 ± 0.005 nb/keV
$\mathcal{L}$	46.1 ± 1.8 pb^{-1}	114.0 ± 4.6 pb^{-1}	114.0 ± 4.6 pb^{-1}
$B_{X\rightarrow\gamma\gamma}$	0.9880 ± 0.0003 (Ref. 1)	0.389 ± 0.004 (Ref. 1)	0.0223 ± 0.0018 (see text)
$\Gamma_{X\rightarrow\gamma\gamma}$	$7.7\pm 0.5\pm 0.5$ eV	$0.514\pm 0.017\pm 0.035$ keV	$4.7\pm 0.5\pm 0.5$ keV

random-trigger events before being analyzed in order to take into account the effect of the machine background. The principal effect of the machine background is to contribute an additional low-energy shower in about 16% of the events and thus cause these events to fail the multiplicity requirement.

The detection efficiency ϵ_{ball} for each of the observed mesons is given in Table I. The detector's geometrical acceptance accounts for most of the inefficiency. The efficiency for events which have two photons satisfying $E_\gamma \geq 40$ MeV, $|\cos\theta| \leq 0.75$, and $|\sum \mathbf{p}_t| \leq \frac{1}{10} M_{\gamma\gamma}$ with no additional requirements and before detector simulation is 5.0%, 8.3%, and 10.7% for π^0, η, and η' events, respectively. The systematic errors shown in Table I for the ball efficiency have been estimated by studying the sensitivity of the final result to variations in the cuts.

The factor $\epsilon_{\text{chamber}}$ has been determined using events of the type $e^+e^- \rightarrow \gamma\gamma(\gamma)$. We first measure the chamber efficiency for the beam-energy photons in these events, and then calculate two small corrections to obtain the chamber efficiency for photons from π^0, η, and η' decays. The $e^+e^- \rightarrow \gamma\gamma(\gamma)$ events are selected in the same way as events used to measure the luminosity. The events are then required to satisfy the same neutrality requirements as the π^0, η, and η' candidates, including the trigger veto on charged particles and the software tracking requirements. We obtain the chamber efficiency by comparing the number of observed events to the number expected based on the acceptance for the showers in the ball, the cross section, and the luminosity. We calculate the cross section and acceptance using a Monte Carlo program by Berends and Kleiss.[25]

We have corrected the chamber efficiency for two energy-dependent effects, both of which increase the acceptance for low-energy photons compared to beam-energy photons. The first effect is the smaller probability for a low-energy photon to convert in the beam pipe or chamber material compared to the probability for a high-energy photon. Using data on the energy dependence of the γ conversion cross section from Hubbell, Gimm, and Overbø,[26] we find an increase in efficiency that ranges from $(0.7\pm0.2)\%$ for η' events in data with six layers of chambers to $(4.0\pm1.1)\%$ for π^0 events with eight layers of chambers.

The second correction required to obtain $\epsilon_{\text{chamber}}$ takes into account the smaller size of photon showers from π^0, η, and η' decays compared to showers from beam-energy photons. The shower size affects the test for straight tracks described in Sec. III, because the projected track is required to pass close to a crystal with ≥ 10 MeV. There are fewer such crystals in a low-energy shower, so the track direction is more restricted. Consequently, noise hits are less likely to fake a straight-line track (according to our criteria) in an event with low-energy showers. By studying the number of events rejected as a function of the number of crystals from each shower used to test the track direction, we have determined that the efficiency is $(2\pm1)\%$ higher for low-energy photons compared to beam-energy photons, with minor variations for the different mesons and chamber configurations.

In addition to the systematic errors for the correction

factors, we estimate a systematic error of 2% for the determination of the chamber efficiency for the beam-energy photons. We have added the three contributions in quadrature to obtain the errors shown in Table I.

The only reason that the requirement on the timing of roof hits is not fully efficient is accidental coincidences. We have studied the probability of such coincidences using the same random triggers discussed above with regard to machine-related energy background. We find that $(0.5\pm0.1)\%$ of the events have a roof hit in the time interval that would cause an event to be rejected. Such events would only be rejected if they also have a recorded time for energy in the bottom hemisphere, which requires at least 130 MeV. None of the π^0 events which satisfy the other selection requirements has this much energy. All of the η and η' events, on the other hand, do. Consequently, this inefficiency contributes only to the η and η' results. For the high-mass analysis, there is the additional requirement that the energy be deposited in the ball consistent with the nominal beam crossing. We have studied the efficiency of this requirement by examining the events that it rejects, but which otherwise satisfy all of the selection requirements. The rejected events are all in the mass range $330 \leq M_{\gamma\gamma} \leq 660$ MeV, with 26 events between 500 and 600 MeV. In a hand scan of the 26 events, 14 ± 4 appear to be genuine collision events, whereas the rest appear to be cosmic-ray events. Since there are approximately 1300 events in the η signal, this implies an efficiency of 0.989 ± 0.003. To summarize, the timing requirements are fully efficient for π^0 events and reject η' events only as a result of accidental coincidences with roof hits. Both roof accidental coincidences and the ball timing requirement contribute small inefficiencies for η events, and the contributions have been combined to obtain the value of ϵ_{TOF} given in Table I.

The final item needed to evaluate the right-hand side of Eq. (5) is the branching ratio $B_{X \rightarrow \gamma\gamma}$. For π^0 and η, the branching ratios are well known and make a small contribution to the systematic error. We take the most recent values (shown in Table I) reported by the Particle Data Group.[1] The resulting values for the two-photon partial widths are

$$\Gamma_{\pi^0 \rightarrow \gamma\gamma} = 7.7\pm0.5\pm0.5 \text{ eV} ,$$

$$\Gamma_{\eta \rightarrow \gamma\gamma} = 0.514\pm0.017\pm0.035 \text{ keV} ,$$

(6)

where we have added the systematic errors for the number of events together in quadrature with the errors for the factors in the denominator of Eq. (5) to obtain the overall systematic errors.

The η' branching ratio is not so well established. For the product of the partial width and branching ratio we obtain

$$\Gamma_{\eta' \rightarrow \gamma\gamma} B_{\eta' \rightarrow \gamma\gamma} = 0.104\pm0.011\pm0.007 \text{ keV} . \qquad (7)$$

The 1986 Particle Data Group value,[1] $B_{\eta' \rightarrow \gamma\gamma} = 0.0185\pm0.0016$, does not include the two most recent published results.[27,28] The average value obtained by including them is 0.0223 ± 0.0018, where we have scaled the error on the average up by 1.8 as described in Ref. 1

to account for disagreement among the experiments. Using this revised value for the branching ratio we derive $\Gamma_{\eta'\to\gamma\gamma}=4.7\pm0.5\pm0.5$ keV.

In comparing experimental results to theoretical models, it is common to use ratios of the two-photon widths of two mesons (cf. Sec. VII). In taking the ratios of widths measured in this experiment, some of the common systematic error cancels. The largest contribution that cancels is the error for the luminosity. In addition, approximately two-thirds of the error for the chamber efficiency and half of the error for the cross section cancels. Adding the remaining systematic errors in quadrature with the statistical errors, we obtain the following ratios:

$$\frac{\Gamma_{\eta\to\gamma\gamma}}{\Gamma_{\pi^0\to\gamma\gamma}}=67\pm6, \quad \frac{\Gamma_{\eta'\to\gamma\gamma}}{\Gamma_{\pi^0\to\gamma\gamma}}=610\pm95 ,$$

$$\frac{\Gamma_{\eta'\to\gamma\gamma}}{\Gamma_{\eta\to\gamma\gamma}}=9.1\pm1.4 . \tag{8}$$

The η' error is dominated by the statistical error and the error for the branching ratio, so the cancellation of part of the error does not make a significant difference for ratios involving the η' width. Without taking the common errors into account for the η-to-π^0 ratio, the result would be 67 ± 8.

VI. SEARCH FOR OTHER RESONANCES

Photon-photon collisions also present an opportunity to search for particles that couple to two photons, but weakly to other known particles. Current theories, in particular the standard model, do not require particles of this type. If they did exist, a particularly good place to find them would be in a study such as this one, which uses photons both for production and for detection of the final state. A resonance coupling only to photons would be expected to be very narrow, so in setting limits we neglect its width compared to our mass resolution. No evidence is found in this experiment for production of any previously unknown narrow resonance. The $\gamma\gamma$ mass spectra in Fig. 2 have been used to calculate upper limits for production of such a resonance.

To determine the cross section, detection efficiency, and resolution for narrow mesons as a function of their mass, we have generated Monte Carlo data samples for $e^+e^-\to e^+e^-X$, $X\to\gamma\gamma$ for 13 hypothetical X masses from 100 to 3000 MeV. We use these samples, together with the Monte Carlo samples for π^0, η, and η' events, to determine the variation of ϵ_{ball}, σ_X, and the mass resolution as a function of the resonance mass m_X. For each of these quantities, we fit a smooth curve to the Monte Carlo points and use values on the curve to calculate the upper limits as a function of m_X.

Upper limits for particles with mass between the π^0 and η masses are obtained using the invariant-mass distribution in Fig. 2(a); limits for $m_X > m_\eta$ are determined using Fig. 2(b). For each tested mass hypothesis, we fit an interval of the invariant-mass distribution with a quadratic background and a peak of fixed mass, fixed

width, and variable amplitude. For mass hypotheses near one of three observed resonances, the contribution of that resonance is included as a second peak of fixed mass, fixed width, and variable amplitude. Each fit result for the amplitude of the peak is used with Eq. (5) to deduce the 90%-confidence-level upper limit for $\Gamma_{X\to\gamma\gamma}B_{X\to\gamma\gamma}$. The limits are shown in Fig. 8 and assume that the meson is spin 0 and decays isotropically. For higher spins, J, the detection efficiency depends on the angular distribution of the decay. Assuming an angular distribution that is still isotropic, the limits are smaller by a factor $(2J+1)^{-1}$ since the cross section $\sigma_{\gamma\gamma\to X}$ is proportional to $(2J+1)$ (Ref. 10).

VII. DISCUSSION

While the π^0, η, and η' partial widths to two photons have all been measured in other experiments, this is the first experiment to simultaneously observe all three of the light pseudoscalars. The results obtained here are listed with other published measurements in Tables II–IV. The other results are obtained using direct measurements of the lifetime combined with the $\gamma\gamma$ branching ratio, the Primakoff effect, or the photon-photon collision technique used in this experiment.

The π^0 results, particularly the more recent ones, are all in agreement with one another. This experiment reports the first observation of π^0 formation in $\gamma\gamma$ collisions, and for the first time a decay width measured with two-photon collisions can be checked against a precise result obtained by a direct measurement of the particle lifetime. There is good agreement between the result from this experiment and the most recent measurement[2] of the π^0 decay length.

The value of $\Gamma_{\eta\to\gamma\gamma}$ from this experiment is the most precise of the measurements using photons from e^+e^- collisions, all of which agree well with each other. However, in this case the photon-photon results do not agree with those obtained with the Primakoff technique. Indeed, the two Primakoff results do not agree with each other. However, the data from the two experiments are in fact consistent.[29] The Cornell result has been quoted (e.g., Ref. 30) as the accepted value until recently (Ref. 1).
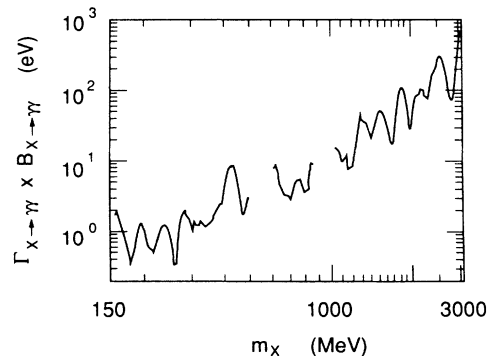

FIG. 8. Upper limits (90% confidence level) for $\Gamma_{X\to\gamma\gamma}B_{X\to\gamma\gamma}$ as a function of m_X for a narrow spin-0 resonance X.

TABLE II. Summary of published experimental results for $\Gamma_{\pi^0 \to \gamma\gamma}$.

$\Gamma_{\pi^0 \to \gamma\gamma}$ (eV)	Technique	Experiment	Reference
6.2 ±1.1	Decay length	von Dardel *et al.*	34
8.9 ±1.3	Primakoff effect	Bellettini *et al.*	35
6.5 ±3.3	Decay length	Stamer *et al.*	36
11.6 ±1.2	Primakoff effect	Bellettini *et al.*	37
7.23±0.55	Primakoff effect	Kryshkin, Sterliov, and Usov	38
7.93±0.39	Primakoff effect	Browman *et al.*	39
7.25±0.23	Decay length	Atherton *et al.*	2
7.7 ±0.5±0.5	$\gamma\gamma$ collisions	This experiment	
7.50±0.17	Average		

Taking the average of the four measurements using photon-photon collisions yields 0.524±0.031 keV for the η partial width. This differs substantially from the Cornell Primakoff measurement, 0.324±0.046 keV.

The η' partial width obtained in this experiment is in agreement with the previous measurements as listed in Table IV, although it is not as precise as other recent measurements, which study decay modes of the η' with larger and better-known branching ratios.

The average values for the partial widths, given in the tables, can be compared to the predictions of the quark model. The quark content of the η and η' is conveniently expressed in terms of a mixing angle θ between the flavor-singlet combination η_0 and the flavor octet η_8:

$$\eta = \eta_8\cos\theta - \eta_0\sin\theta, \quad \eta' = \eta_8\sin\theta + \eta_0\cos\theta , \tag{9}$$

where

$$\eta_0 = \frac{1}{\sqrt{3}}(\, |u\bar{u}\rangle + |d\bar{d}\rangle + |s\bar{s}\rangle) ,$$

$$\eta_8 = \frac{1}{\sqrt{6}}(\, |u\bar{u}\rangle + |d\bar{d}\rangle - 2|s\bar{s}\rangle) . \tag{10}$$

In principle there are many other states that might be mixed into the η and η'. They include heavy-quark states such as the η_c, radial excitations of the light-quark states, and gluonia, bound state of two gluons. We neglect such states here in order to consider whether the mixing of the states η_0 and η_8 alone can account for the measured two-photon widths. The calculation of the partial widths for the states π^0, η_0, and η_8 using current algebra yields the relations[31]

$$\frac{\Gamma_{\eta \to \gamma\gamma}}{\Gamma_{\pi^0 \to \gamma\gamma}} = \frac{1}{3}\frac{m_\eta^3}{m_\pi^3}\left[\frac{f_\pi\cos\theta}{f_8} - \frac{\sqrt{8}f_\pi\sin\theta}{f_0} \right]^2 ,$$

$$\frac{\Gamma_{\eta' \to \gamma\gamma}}{\Gamma_{\pi^0 \to \gamma\gamma}} = \frac{1}{3}\frac{m_{\eta'}^3}{m_\pi^3}\left[\frac{f_\pi\sin\theta}{f_8} + \frac{\sqrt{8}f_\pi\cos\theta}{f_0} \right]^2 . \tag{11}$$

The pion decay constant f_π is 93 MeV, and f_0 and f_8 are the decay constants for the quark combinations η_0 and η_8. The ratio $f_8/f_\pi \approx 1.25$ has been calculated using chiral perturbation theory.[32] We use this value and the experimental averages to determine the mixing angle from Eqs. (11). We find

$$\theta = -22.4° \pm 1.2°, \quad f_\pi/f_0 = 0.95 \pm 0.02 . \tag{12}$$

If we use only the results from this experiment, Eq. (8), then we find $\theta = -21.0° \pm 2.1°$ and $f_\pi/f_0 = 0.97 \pm 0.06$. Gilman and Kauffman[33] have recently evaluated experimental data for several properties of η and η' mesons using the mixing scheme in Eq. (9), and find that all of the data are compatible with a mixing angle $\theta \approx -20°$. Thus, there is no apparent need for mixing with other states.

In conclusion, we report new measurements of the two-photon partial widths of π^0, η, and η'. This is the first time that formation of π^0s in two-photon collisions has been observed. The agreement of $\Gamma_{\pi^0 \to \gamma\gamma}$ obtained here with the value derived from a measurement of the decay length checks the technique of using colliding e^+e^- beams as photon sources and is the first confirmation that partial widths measured by the two techniques agree. The value of $\Gamma_{\eta \to \gamma\gamma}$ from this experiment is the most precise measurement of that quantity to

TABLE III. Summary of published experimental results for $\Gamma_{\eta \to \gamma\gamma}$.

$\Gamma_{\eta \to \gamma\gamma}$ (keV)	Technique	Experiment	Reference
1.00 ±0.22	Primakoff effect	DESY	40
0.324±0.046	Primakoff effect	Cornell	29
0.56 ±0.12±0.10	$\gamma\gamma$ collisions	Crystal Ball (SPEAR)	41
0.53 ±0.04±0.04	$\gamma\gamma$ collisions	JADE	42
0.64 ±0.14±0.13	$\gamma\gamma$ collisions	TPC/$\gamma\gamma$	43
0.514±0.017±0.035	$\gamma\gamma$ collisions	This experiment	
0.524±0.031	Average of $\gamma\gamma$ collision results		

TABLE IV. Summary of published experimental results for $\Gamma_{\eta' \to \gamma\gamma}$. All of the results use photon-photon collisions, except for Binnie et al., who measured the width of the η' missing mass peak in the process $\pi^- p \to n +$ unseen. The two-photon width has been obtained from their full width using the branching ratio $B_{\eta' \to \gamma\gamma}$. For the other measurements, the decay mode used to reconstruct η' events is given.

$\Gamma_{\eta' \to \gamma\gamma}$ (keV)	Decay mode	Experiment	Reference
6.2 ±2.3		Binnie et al.	44
5.8 ±1.1±1.2	$\rho\gamma$	Mark II (SPEAR)	45
5.0 ±0.5±0.9	$\rho\gamma$	JADE	46
6.2 ±1.1±0.8	$\rho\gamma$	CELLO	47
5.1 ±0.4±0.7	$\rho\gamma$	TASSO	48
3.80±0.26±0.43	$\rho\gamma$	PLUTO	13
3.3 ±0.7	$\gamma\gamma$	JADE	42
4.5 ±0.3±0.7	$\rho\gamma$	TPC/$\gamma\gamma$	14
4.7 ±0.7±0.9	$\eta\pi^+\pi^-$, $\eta \to \gamma\gamma$	Mark II (PEP)	15
4.6 ±0.4±0.6	$\eta\pi^0\pi^0 \to 6\gamma$	Crystal Ball (DORIS)	23
3.76±0.13±0.47	$\rho\gamma$	Argus	49
4.7 ±0.5±0.5	$\gamma\gamma$	This experiment	
4.28±0.22	Average		

date. With one exception, the results for π^0, η, and η' reported here are in agreement with other experiments. The exception is that the values of $\Gamma_{\eta \to \gamma\gamma}$ measured in photon-photon collisions agree well with each other, but disagree with a measurement using the Primakoff technique. The η-η' mixing angle derived from the two-photon widths is about $-22°$, which is consistent with values obtained from other properties of the pseudoscalars.

Note added in proof. The 1988 Particle Data Group value for $B_{\eta' \to \gamma\gamma}$ is 0.0216±0.0016 (Ref. 50), where the error includes a scale factor of 1.4 to account for disagreement among the experiments. If we use this value, we obtain a partial width $\Gamma_{\eta' \to \gamma\gamma} = 4.8±0.5±0.5$ keV from this experiment, nearly unchanged from the value given above.

ACKNOWLEDGMENTS

[a]Present address: Massachusetts Institute of Technology, Cambridge, MA 02139.
[b]Present address: Universität München, München, Germany.
[c]Present address: CERN/EP, Geneva, Switzerland.
[d]Present address: Institute for Particle Physics, University of California, Santa Cruz, CA 95064.
[e]Present address: Nuclear Physics Laboratory, Oxford University, Keble Road OX1 3RH, England.
[f]Present address: Max Planck Institute, München, Germany.
[g]Present address: Lawrence Berkeley Laboratory, Berkeley, CA 94720.
[h]Present address: III. Physikalisches Institut A, Rheinisch-Westfälische Technische Hochschule, Aachen, Germany.
[i]Permanent address: Département de Physique des Particules Elémentaires, Centre d'Etudes Nucléaires de Saclay, Gif-sur-Yvette, France.

[1]Particle Data Group, M. Aguilar-Benitez et al., Phys. Lett. 170B, 1 (1986).
[2]H. Atherton et al., Phys. Lett. 158B, 81 (1985).
[3]More information about this analysis can be found in D. Willi-

ams, Ph. D. thesis, Harvard University, 1987.

[4]F. Low, Phys. Rev. **120**, 582 (1960).

[5]E. D. Bloom and C. W. Peck, Annu. Rev. Nucl. Part. Sci. **33**, 143 (1983); M. Oreglia *et al.*, Phys. Rev. D **25**, 2259 (1982).

[6]The measured energy E_{meas} of each photon has been corrected using the formula $E_{corr} = E_{meas}/[1 + 0.0137 \ln(E_{meas}/E_{beam})]$. The use of this formula correctly gives the π^0 mass and the mass difference $m_{\Upsilon(2S)} - m_{\Upsilon(1S)}$ in the reaction $\Upsilon(2S) \to \pi^0\pi^0\Upsilon(1S)$, which were otherwise about 5% too low. The need for a correction stems from the extrapolation of the calibration energy (5 GeV from Bhabha events) down to the energy range 20–300 MeV. A discussion of this effect, and derivation of the form of the correction, can be found in D. Gelphman, Ph.D. thesis, Stanford University, 1985 (SLAC Report No. 286).

[7]For more detail about the roof counters, see D. Prindle, Ph.D. thesis, Carnegie-Mellon University, 1985.

[8]For this preliminary step, the transverse-momentum sum is calculated by assigning a momentum vector to each crystal with magnitude equal to the energy detected in that crystal. At all other stages of the analysis, transverse momentum is calculated from the reconstructed energies and direction of the showers.

[9]For preliminary results on the first observation of this process, see D. Williams, in *Proceedings of the XXIII International Conference on High Energy Physics,* Berkeley, California, 1986, edited by S. Loken (World Scientific, Singapore, 1987), p. 1223 and H. Marsiske, contributed paper to that conference.

[10]See, e.g., H. Kolanoski, *Two-Photon Physics at e^+e^- Storage Rings* (Springer, Berlin, 1984); M. Poppe, Int. J. Mod. Phys. **1**, 545 (1986).

[11]G. Köpp, T. Walsh, and P. Zerwas, Nucl. Phys. **B70**, 461 (1974).

[12]The average values of $(-q^2)$ for accepted Monte Carlo events are 10 MeV^2 for π^0 events, 175 MeV^2 for η events, and 760 MeV^2 for η' events.

[13]PLUTO Collaboration, Ch. Berger *et al.* Phys. Lett. **142B**, 125 (1984).

[14]TPC/$\gamma\gamma$ Collaboration, H. Aihara *et al.*, Phys. Rev. D **35**, 2650 (1987).

[15]Mark II Collaboration, G. Gidal *et al.*, Phys. Rev. Lett. **59**, 2012 (1987).

[16]J. Vermaseren, Nucl. Phys. **B229**, 347 (1983).

[17]D. Dicus, Phys. Rev. D **15**, 2524 (1977).

[18]M. Defrise *et al.*, Phys. Rev. D **23**, 663 (1981); W. van Neerven and J. Vermaseren, Nucl. Phys. **B238**, 73 (1984); Phys. Lett. **142B**, 80 (1984).

[19]J. Gaiser *et al.*, Phys. Rev. D **34**, 711 (1986); J. Gaiser, Ph.D. thesis, Stanford University, 1983 (SLAC Report No. 255); R. Lee, Ph.D. thesis, Stanford University, 1985 (SLAC Report No. 282).

[20]For decays of slow particles, the opening angle is large and the mass resolution is dominated by the energy resolution. For typical π^0 decays in multihadron events, the mass resolution is dominated by the resolution in the opening angle, and we observe an invariant-mass peak which is Gaussian.

[21]R. Ford and W. Nelson, SLAC Report No. 210, 1978 (unpublished).

[22]K. Wachs, Ph.D. thesis, Hamburg University, 1988 (DESY Report No. F31-88-01).

[23]D. Antreasyan *et al.*, Phys. Rev. D **36**, 2633 (1987).

[24]Approximately 15% of the crystals were affected by this problem. The errors were restricted to true energies greater than 280 MeV in a single crystal, and for most of the affected crystals, a very limited energy range was recorded incorrectly. Since photons deposit roughly 70% of their energy in one crystal, this implies that photons with less than 400 MeV are rarely affected. The problem was in the read-out electronics and was subsequently studied with a pulse generator, so that its effect could be included in the Monte Carlo detector simulation. It is discussed in more detail in S. Lowe, Ph.D. thesis, Stanford University, 1986 (SLAC Report No. 307).

[25]F. Berends and R. Kleiss, Nucl. Phys. **B186**, 22 (1981).

[26]J. Hubbell, H. Gimm, and I. Overbø, J. Phys. Chem. Ref. Data **9**, 1023 (1980).

[27]N. Stanton *et al.*, Phys. Lett. **92B**, 353 (1980). The result in this paper includes the data of W. Apel *et al.*, *ibid.* **83B**, 131 (1979) and Nucl. Phys. **B152**, 1 (1979).

[28]D. Alde *et al.*, Z. Phys. C **36**, 603 (1987).

[29]A. Browman *et al.*, Phys. Rev. Lett. **32**, 1067 (1974).

[30]Particle Data Group, C. G. Wohl *et al.*, Rev. Mod. Phys. **56**, S1 (1984). Earlier editions [e.g., Phys. Lett. **75B**, 51 (1978)] contain a note discussing the reason the result of Ref. 40 is not included in the average.

[31]See, e.g., M. Chanowitz, in *Proceedings of the 6th International Workshop on Photon-Photon Collisions,* Lake Tahoe, California, 1984, edited by R. Lander (World Scientific, Singapore, 1985), p. 95.

[32]J. Donoghue, B. Holstein, and Y.-C. Lin, Phys. Rev. Lett. **55**, 2766 (1985); J. Gasser and H. Leutwyler, Nucl. Phys. **B250**, 465 (1985); see also G. Grunberg, Phys. Lett. **168B**, 141 (1986).

[33]F. Gilman and R. Kauffman, Phys. Rev. D **36**, 2761 (1987).

[34]G. von Dardel *et al.*, Phys. Lett. **4B**, 51 (1963).

[35]G. Bellettini *et al.*, Nuovo Cimento **40A**, 1139 (1965).

[36]P. Stamer *et al.*, Phys. Rev. **151**, 1108 (1966).

[37]G. Bellettini *et al.*, Nuovo Cimento **66A**, 243 (1970).

[38]V. Kryshkin, A. Sterliov, and Yu. Usov, Zh. Eksp. Teor. Fiz. **57**, 1917 (1969) [Sov. Phys. JETP **30**, 1037 (1970)].

[39]A. Browman *et al.*, Phys. Rev. Lett. **33**, 1400 (1974).

[40]C. Bemporad *et al.*, Phys. Lett. **25B**, 380 (1967). We have corrected the value of $\Gamma_{\eta \to \gamma\gamma}$ to account for the most recent value of the $\eta \to \gamma\gamma$ branching ratio in Ref. 1.

[41]Crystal Ball Collaboration, A. Weinstein *et al.*, Phys. Rev. D **28**, 2896 (1983).

[42]JADE Collaboration, W. Bartel *et al.*, Phys. Lett. **160B**, 421 (1985). The value of $\Gamma_{\eta' \to \gamma\gamma}$ from this paper has been scaled to reflect the revised value of the branching ratio $B\eta' \to \gamma\gamma$, discussed in Sec. V.

[43]TPC/$\gamma\gamma$ Collaboration, H. Aihara *et al.*, Phys. Rev. D **33**, 844 (1986).

[44]D. Binnie *et al.*, Phys. Lett. **83B**, 141 (1979). The value of $\Gamma_{\eta' \to \gamma\gamma}$ from this paper has been scaled to reflect the revised value of the branching ratio $B_{\eta' \to \gamma\gamma}$, discussed in Sec. V.

[45]Mark II Collaboration, G. Abrams *et al.*, Phys. Rev. Lett. **43**, 477 (1979); P. Jenni *et al.*, Phys. Rev. D **27**, 1031 (1983).

[46]JADE Collaboration, W. Bartel *et al.*, Phys. Lett. **113B**, 190 (1982).

[47]CELLO Collaboration, H. Behrend *et al.*, Phys. Lett. **114B**, 378 (1982); **125B**, 518(E) (1983).

[48]TASSO Collaboration, M. Althoff *et al.*, Phys. Lett. **147B**, 487 (1984).

[49]Argus Collaboration, H. Albrecht *et al.*, Phys. Lett. B **199**, 457 (1987).

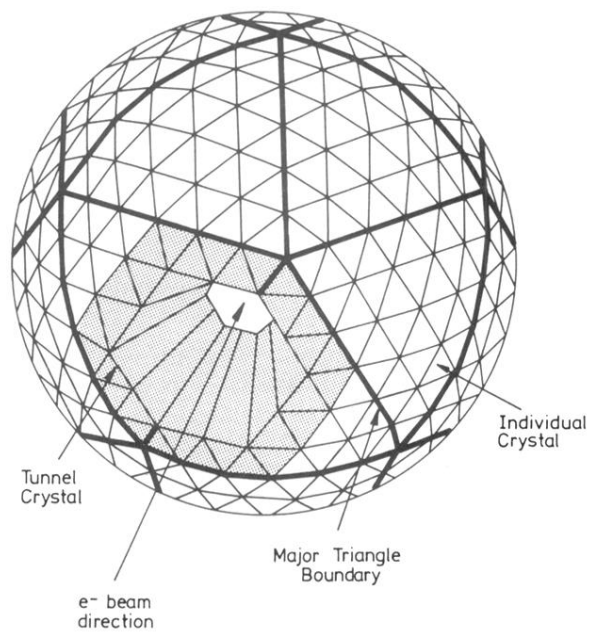[50]Particle Data Group, G. Yost *et al.*, Phys. Lett. B **204**, 1 (1988).

FIG. 1. The organization of the Crystal Ball into major triangles. The shaded area is one of the "tunnel regions" next to the beam.